Biochimica et Biophysica Acta 1818 (2012) 448–457

Contents lists available at SciVerse ScienceDirect

Biochimica et Biophysica Acta

journal homepage: www.elsevier.com/locate/bbamem

Cellular uptake and biophysical properties of galactose and/or tryptophan containing cell-penetrating peptides

Pascaline Lécorché [a,b,c,1], Astrid Walrant [a,b,c,1], Fabienne Burlina [a,b,c], Laurence Dutot [a,b,c], Sandrine Sagan [a,b,c], Jean-Maurice Mallet [a,b,c], Bernard Desbat [d], Gérard Chassaing [a,b,c], Isabel D. Alves [a,b,d], Solange Lavielle [a,b,c,*]

[a] UPMC-Univ Paris06, UMR 7203, Laboratoire des BioMolécules, Université P. et M. Curie 4, Place Jussieu, 75005 Paris, France
[b] CNRS, UMR 7203, France
[c] ENS, UMR 7203, Département de Chimie, Ecole Normale Supérieure, 24, Rue Lhomond 75005 Paris, France
[d] CBMN, UMR CNRS 5248, Université Bordeaux, IPB, All. Geoffroy Saint-Hilaire 33600 Pessac, France

ARTICLE INFO

Article history:
Received 28 September 2011
Received in revised form 28 November 2011
Accepted 5 December 2011
Available online 13 December 2011

Keywords:
Cell penetrating peptide
Internalization
Glycosylation
Microcalorimetry
Tryptophan
MALDI-TOF mass-spectrometry

ABSTRACT

Glycosylated cell penetrating peptides (CPPs) have been conjugated to a peptide cargo and the efficiency of cargo delivery into wild type Chinese hamster ovary (CHO) and proteoglycan deficient CHO cells has been quantified by MALDI-TOF mass spectrometry and compared to tryptophan- or alanine containing CPPs. In parallel, the behavior of these CPPs in contact with model membranes has been characterized by different biophysical techniques: Differential Scanning and Isothermal Titration Calorimetries, Imaging Ellipsometry and Attenuated Total Reflectance IR spectroscopy. With these CPPs we have demonstrated that tryptophan residues play a key role in the insertion of a CPP and its conjugate into the membrane: galactosyl residues hampered the internalization when introduced in the middle of the amphipathic secondary structure of a CPP but not when added to the *N*-terminus, as long as the tryptophan residues were still present in the sequence. The insertion of these CPPs into membrane models was enthalpy driven and was related to the number of tryptophans in the sequence of these secondary amphipathic CPPs. Additionally, we have observed a certain propensity of the investigated CPP analogs to aggregate in contact with the lipid surface.

1. Introduction

Cell penetrating peptides (CPPs) with their capacity to shuttle cargoes inside cells are regarded as a sort of "magic bullets" for intracellular delivery of bioactive molecules, even though their intracellular localization is dependent on their mechanism(s) of entrance: direct translocation of the plasma membrane or endocytotic pathways [1–6]. In search of some specificity in addressing CPPs, we have studied the effect of CPP myristoylation on the delivery of a peptide cargo. Myristoylation of commonly used CPPs and synthetic dendrimers showed an increase in conveying a cargo inside CHO cells [7,8]. Recently, we have explored the influence of glycosylation of a CPP sequence on cargo delivery, taking as a starting point our lead CPP: Ac-RRWWRRWRR-NH_2 [9]. Glycosylation of bioactive compounds has been used mainly for increasing the hydrophilicity, the enzymatic stability, and/or the delivery into the brain [10–12]. In the context of CPPs, we have hypothesized that glycosylation could regulate the binding to the plasma membrane of CPPs and conjugates and consequently their internalization pathway and/or specificity.

In our previous study, the pro-apoptotic KLAK peptide $(KLAKLAK)_2$, was conjugated via a labile disulfide linker to analogs of the CPP Ac-C-RRWWRRWRR-NH_2, these analogs possessing galactosyl unit(s) instead of the indole side-chains of the tryptophans [13]. Cell viability studies showed an inverse relationship with the number of galactosyl moieties, the conjugate, Ac-C-RRA(βtGal)A(βtGal)RRA(βtGal)RR-NH_2, with three galactoses and no tryptophan, did not induce CHO cell death. Furthermore, fluorescence studies performed in parallel showed that the KLAK peptide was not delivered inside the cells with this galactosyl-substituted peptide. This correlation between cell death and cellular uptake of the cargo was also observed for the other glycosylated vectors studied [13]. Rothbard et al. have shown that analogs of

Abbreviations: ATR Spectroscopy, Attenuated Total Reflection Spectroscopy; CPP, cell-penetrating peptide; CHO, Chinese hamster ovary; DIPEA, diisopropylethylamine; DMF, dimethylformamide; DMPC, dimyristoylphosphatidylcholine; DMPG, dimyristoylphosphatidylglycine; DSC, differential scanning calorimetry; DSPG, distearylphosphatidylglycine; GAG, glycosaminoglycan; DMEM, Dulbecco's modified Eagle's medium; ITC, isothermal titration calorimetry; KLAK peptide, $(KLAKLAK)_2$; LUVs, large unilamellar vesicles; MALDI-TOF, matrix-assisted laser desorption ionization time-of-flight; MLVs, multilamellar vesicles; MS, mass spectrometry; NMP, *N*-methylpyrrolidone; PKCi, peptide inhibitor of protein kinase C; RP-HPLC, reverse-phase high-pressure chromatography; RT, room temperature; TFA, trifluoroacetic acid; TIS, triisopropylsilane.

* Corresponding author at: Laboratoire des BioMolécules, UMR 7203 UPMC-CNRS-ENS, Département de Chimie, Ecole Normale Supérieure, 24, Rue Lhomond, 75005 Paris, France. Tel.: +33 1 44 32 24 43; fax: +33 1 44 32 24 02.
E-mail address: solange.lavielle@upmc.fr (S. Lavielle).
[1] These authors contributed equally to this work and should be considered as joint first authors.

0005-2736/$ – see front matter © 2011 Elsevier B.V. All rights reserved.
doi:10.1016/j.bbamem.2011.12.003

$(Arg)_{10}$ were as efficient as $(Arg)_{10}$ to enter Jurkat cells when simultaneously modified in positions 2, 5 and 8 by proteinogenic or modified amino acids (Trp and Cys were not tested), except the two analogs with acidic residues: Arg_7/Asp_3 and Arg_7/Glu_3, which "entered cells relatively poorly" [14]. The aim of the present study was to aid in the identification of the structural, physico-chemical and thermodynamic parameters relevant for cellular uptake. For this, we have quantified the efficiency of cargo delivery of glycosylated CPPs into cells and analyzed by different techniques their interactions with model membranes. The glycosylated CPPs studied previously ((**3**) and (**4**), (Table 1)) were conjugated to a peptide inhibitor of protein kinase C (PKCi) [7,15–17]. We have also synthesized a new glycosylated CPP (**5**) with three galactose units on the *N*-terminus of the Arg/Trp sequence, and a control Arg/Ala peptide (**2**), suspecting that tryptophan residues were playing an essential role in the internalization process.

Herein, we report the quantification by MALDI-TOF mass spectrometry [18,19] of the PKCi cargo internalized into wild type CHO and proteoglycan deficient CHO cells [4]. Indeed many studies showed that CPPs bind to glycosaminoglycans (GAGs) with significant affinity [20–22] and that GAGs are involved in CPPs internalization pathways [4,23]. In parallel, we have characterized by different biophysical techniques (DSC, ITC, Imaging Ellipsometry and ATR) the behavior of the glycosylated CPPs in contact with LUVs and lipid monolayers. Our results show a clear correlation between the efficiency of internalization, the presence of tryptophan residues on the CPP sequence and an enthalpy gain resulting from the energetically favorable transfer of Trp residues from the aqueous solution to the interior of the lipid bilayer.

2. Material and methods

2.1. Peptide syntheses

Rink amide (*p*-methylbenzhydrylamine)-resin (MBHA-resin, 100–200 mesh), (4-(2′-4′-dimethoxyphenyl-Fmoc-aminomethyl)-phenoxyacetamido-norleucyl-MBHA polystyrene resin, 0.64 mmol/g), *O*-(benzotriazol-1-yl)-1,1,3,3-tetramethyluronium hexafluorophosphate (HBTU), Fmoc-Cys(*S*-*St*Bu)-OH, Fmoc-Arg(Pbf)-OH, Fmoc-Trp(Boc)-OH and Fmoc-Ala-OH were purchased from Novabiochem. Fmoc-Pra-OH was purchased from IRIS Biotech. Peptides were characterized by MALDI-TOF MS (DE-Pro, ABI) in positive ion reflector mode using the matrix CHCA. The m/z of the protonated molecules is given as experimental and calculated in Table 2. Proteomix 4 (Laserbio Labs) [500–3500 Da] was used for calibration.

Table 1
Sequences of the cell-penetrating peptides and the corresponding PKCi conjugates.

N°	Sequence
(**1**)	Ac-C(*S*-Acm)*RRWWRRWRR-NH$_2$*
(**2**)	Ac-C(*S*-Acm)*RRAARRARR-NH$_2$*
(**3**)	Ac-C(*S*-Acm)*RRWA(βtGal)RRWRR-NH$_2$*
(**4**)	Ac-C(*S*-Acm)*RRA(βtGal)A(βtGal)RRA(βtGal)RR-NH$_2$*
(**5**)	Ac-*A(βtGal)A(βtGal)A(βtGal)*C(*S*-Acm) *RRWWRRWRR-NH$_2$*
(**1′**)	Biot(O_2)-GGGGC(S-S(*NAc*)*CRRWWRRWRR-NH$_2$*)-RFARKGALRQKNV-NH_2
(**2′**)	Biot(O_2)-GGGGC(S-S(*NAc*)*CRRAARRARR-NH$_2$*)-RFARKGALRQKNV-NH_2
(**3′**)	Biot(O_2)-GGGGC(S-S(*NAc*)*CRRWA(βtGal)RRWRR-NH$_2$*)-RFARKGALRQKNV-NH_2
(**4′**)	Biot(O_2)-GGGGC(S-S(*NAc*)*CRR(βtGalA)(βtGalA)RR(βtGalA)RR-NH$_2$*)-RFARKGALRQKNV-NH_2
(**5′**)	Biot(O_2)GGGGC(S-S(*NAc-A(βtGal)A(βtGal)A(βtGal))CRRWWRRWRRNH$_2$*)-RFARKGALRQKNV-NH_2

Acm: $-CH_2-C(O)-NH_2$; Biot(O_2): biotine sulfone; A(βtGal): β-(1H,3-galactosyl-[1-3] triazol)alanine and PKCi: RFARKGALRQKNV. CPP sequences are represented in italic in the table for a better visualization within the sequences of the conjugates with PKCi.

2.1.1. Ac-C-RRAARRARR-NH_2

Ac-C(*S*-*St*Bu)-RRAARRARR-NH_2 was synthesized manually by solid-phase methodology on a Rink amide resin (0.64 mmol/g) by Fmoc strategy in a fritted syringe. Fmoc protection was removed with a solution of piperidine in NMP (20%, 3×5min). Stepwise coupling reactions were performed with Fmoc-protected amino acids, HBTU and DIPEA (3/2.85/3 eq) at RT. After removal of the last Fmoc protecting group, the peptide was *N*-acetylated with a solution of acetic anhydride in NMP (20%, 45 min). The resin was washed with NMP, CH_2Cl_2, CH_3OH and dried under *vacuum*. The resin was then treated with TFA/H_2O/TIS: 95/2.5/2.5 (15 mL/g resin, 2 h, RT), the cleaved peptide precipitated in diethyl ether, lyophilized and purified by RP-HPLC on a preparative C8 column using a 30 min linear methanol (0.1% TFA) gradient in an aqueous solution (0.1% TFA) to yield the product as a white powder after lyophilisation (20% yield). The purity of the peptide was determined by analytical RP-HPLC on a C8 column using a linear methanol (0.1% TFA) gradient in an aqueous solution (0.1% TFA). Retention time of the product was 15.7 min (0–100% methanol over 30 min). The peptide was characterized by MALDI-TOF MS: (m/z) $[MH]^+$ calcd 1400.80, found 1400.90.

DTT (20 eq) was added to Ac-C(*S*-*St*Bu)-RRAARRARR-NH_2, dissolved in a degassed solution of Tris–HCl 50 mM (~2 mM), and the reaction was stirred at RT for 2 h. The reaction was monitored by RP-HPLC. Crude thiol peptide was then purified by RP-HPLC on a preparative C8 column using a linear methanol (0.1% TFA) gradient in an aqueous solution (0.1% TFA) to yield the product as a white powder after lyophilisation (9% yield). Peptide purity was analyzed by analytical RP-HPLC on a C8 column using a linear methanol (0.1% TFA) gradient in an aqueous solution (0.1% TFA). Retention time of the product was 9.8 min (0–100% methanol over 30 min). The peptide was characterized by MALDI-TOF MS: (m/z) $[MH]^+$ calcd 1312.76, found 1312.56.

2.1.2. Ac-A(βtGal)A(βtGal)A(βtGal)-C-RRWWRRWRR-NH_2

Ac-Pra-Pra-Pra-C(*S*-*St*Bu)-RRWWRRWRR-NH_2 was synthesized manually by solid-phase methodology on a Rink amide resin (0.64 mmol/g) by Fmoc strategy in a fritted syringe. Fmoc protection was removed with a solution of piperidine in NMP (20%, 3×5 min). Stepwise coupling reactions were performed with Fmoc-protected amino acids, HBTU and DIPEA (3/2.85/3 eq) at RT. After removal of the last Fmoc protecting group, the peptide was *N*-acetylated with a solution of acetic anhydride in NMP (20%, 45 min). The resin was washed with NMP, CH_2Cl_2, MeOH and dried under vacuum. For analysis, approximately 5 mg of the resin was treated with TFA/H_2O/TIS: 95/2.5/2.5 (15 mL/g resin, 2 h, RT), the peptide precipitated in diethyl ether, lyophilized and analyzed by analytical RP-HPLC on a C8 column using a linear methanol (0.1% TFA) gradient in an aqueous solution (0.1% TFA). Retention time of the product was 9.8 min (0–100% methanol over 30 min). The pure peptide was characterized by MALDI-TOF MS (m/z) [MH] + calcd 2031.04, found 2031.1.

In a fritted syringe CuI (15 eq), ascorbic acid (15 eq), the azido-sugar: 1-azido-2,3,4,6-tetra-*O*-acetyl-β-(D)-galactopyranoside (6 eq) [13] and a degassed solution of DMF(anhydrous)/2,6-lutidine (7/3) containing DIPEA (21 eq) were added to the dried Pra containing-peptidyl-resin, Ac-Pra-Pra-Pra-C(*S*-*St*Bu)-RRWWRRWRR-resin (0.023 M). The solution was sonicated for 5 min and shaken for 15 h at RT. The resin was then washed with DMF, DMF/Pyridine (6/5) containing ascorbic acid (0.02 g/mL), CH_2Cl_2 and MeOH. The resin was dried under vacuum and then cleaved using TFA/H_2O/TIS: 95/2.5/2.5. Analytical RP-HPLC showed complete conversion of the peptide into the glycopeptide. The major peak in the HPLC spectra was identified as the expected product. RP-HPLC retention time of the crude product was ~16.5 min (30–100% methanol over 30 min). MALDI-TOF MS: (m/z) $[MH]^+$ calcd 3150.37, found 3150.56. This peptide, Ac-A(βtGal(*OAc*))A(βtGal(*OAc*)A(βtGal(*OAc*))-C(*S*-*St*Bu)-RRWWRRWRR-NH_2 was used directly for the next step.

Table 2
Characterization of cell-penetrating peptides (**1**–**5**) and conjugates (**1′**–**5′**).

N°	Yield[a]	RP-HPLC, retention time gradient[b]	MALDI-TOF MS (m/z) $[M,H]^+$ (*calculated*)[c]
(**1**)	57%	16.2 min (0–100% MeOH)	$[M,H]^+$: 1714.91 (*calc. 1714.91*)
(**2**)	51%	8.5 min (0–100% MeOH)	$[M,H]^+$: 1369.77 (*calc. 1369.79*)
(**3**)	40%	14.5 min (0–100% MeOH)	$[M,H]^+$: 1829.32 (*calc. 1828.94*)
(**4**)	60%	8.2 min (0–100% MeOH)	$[M,H]^+$: 2057.15 (*calc. 2056.99*)
(**5**)	26%	18 min (0–100% MeOH)	$[M,H]^+$: 2615.96 (*calc. 2615.23*)
(**1′**)	51%	14.6 min (0–60% MeCN)	[Ac-C(SH)RRWWRRWRR,H]$^+$: 1657.54 (*calc. 1657.89*); [PKCi-SH,H]$^+$: 2132.37 (*calc. 2132.10*)
(**2′**)	47%	15.8 min (0–100% MeOH)	Ac-C(SH)RRAARRARR, H]$^+$: 1312.20 (*calc. 1312.76*); [PKCi-SH,H]$^+$: 2131.68 (*calc. 2132.10*)
(**3′**)	45%	14.7 min (0–100% MeOH)	[Ac-C(SH)RRWA(βtGal)RRWRR,H]$^+$: 1772.77 (*calc. 1772.93*); [PKCi-SH,H]$^+$: 2131.96 (*calc. 2132.10*)
(**4′**)	51%	11.0 min (0–100% MeOH)	[Ac-C(SH)RRA(βtGal)A(βtGal)RRA(βtGal)RR,H]$^+$: 1999.98 (*calc. 1999.97*); [PKCi-SH,H]$^+$: 2132.10 (*calc. 2132.10*)
(**5′**)	54%	13.9 min (0–60% MeCN)	[Ac-A(βtGal)A(βtGal)A(βtGal)C(SH)RRWWRRWRR,H]$^+$: 2557.40 (*calc. 2558.21*); [PKCi-SH,H]$^+$: 2131.57 (*calc. 2132.10*)

[a] The yields reported herein correspond to the last step: protection of the thiol function for peptides (**1**–**5**) and coupling with the PKCi cargo for peptides (**1′**–**5′**) and the subsequent RP-HPLC purification.
[b] (min) linear gradient over 30 min as indicated.
[c] The value reported in italic between brackets corresponds to the calculated mass as $[M,H]^+$.

The *O*-acetyl protecting groups of Ac-A(βtGal(*O*Ac))A(βtGal(*O*Ac)A(βtGal(*O*Ac))-C(*S*-*St*Bu)-RRWWRRWRR-NH_2 were removed with a solution of NH_4OH (28%) in THF/MeOH (1/2/2, HO^- concentration ~7 mM). The reaction was followed until its completion by RP-HPLC using a linear methanol (0.1% TFA) gradient in an aqueous solution (0.1% TFA). RP-HPLC showed two main products corresponding to the deacetylated peptides with different amounts of the Cys(*S*-*St*Bu) and the deprotected cysteine. After evaporation of THF and CH_3OH and lyophilization of the residual aqueous solution, the mixture of peptides (corresponding to the presence of the deprotected and the protected cysteine Cys*S*-*St*Bu) was dissolved in a degassed solution of Tris–HCl 50 mM (~2 mM). DTT (20 eq) was added and the reaction was stirred at RT for 2 h. Ac-A(βtGal)A(βtGal)A(βtGal)-C-RRWWRRWRR-NH_2 was purified by RP-HPLC on a preparative C8 column using a linear methanol (0.1% TFA) gradient in an aqueous solution (0.1% TFA). Peptide purity was analyzed by analytical RP-HPLC with a C8 column using a linear acetonitrile (0.1% TFA) gradient in an aqueous solution (0.1% TFA). Retention time of the product was 17.0 min (0–100% methanol over 30 min). The peptide was characterized by MALDI-TOF MS: (m/z) $[MH]^+$ calcd 2558.21, found 2557.76. Overall yield (peptide synthesis, click chemistry, deacetylation, Cys(*S*-*St*Bu) deprotection and purification) was 1.8%.

2.1.3. Syntheses of peptides (**1**–**5**)

To a solution (~1–2 mM) of the different CPP, with a deprotected cysteine, dissolved under argon in carefully degassed Tris–HCl (50 mM) were added TCEP (3 eq) and iodoacetamide (50 eq). The solutions were then homogenized using an argon flux (bubbling for 3 min) and air above the reaction mixture was saturated with argon. After stirring in the dark, completion of the reactions were determined by HPLC monitoring. The retention times of the starting and expected peptides were quite similar and co-injection was often necessary to be sure of the peak identification. The peptides were purified by RP-HPLC with a C8 column using a linear acetonitrile or methanol (0.1% TFA) gradient in an aqueous solution (0.1% TFA). Peptides were analyzed by analytical RP-HPLC with a C8 column using a linear acetonitrile or methanol (0.1% TFA) gradient in an aqueous solution (0.1% TFA) and characterized by MALDI-TOF MS (m/z).

2.1.4. Syntheses of the conjugates (**1′**–**5′**)

The CPPs with a SH-free cysteine, prepared as described above for the obtention of peptides (**1**) and **(5)**, were dissolved under argon bubbling in a carefully degassed 10% acetic acid solution and mixed with a slight excess (1.2 eq) of peptide Biot(O_2)-GGGG-C(Npys)-RFARKGALRQKNV-NH_2. Completions of the reactions were monitored by RP-HPLC. Usually reaction times comprised between 12 h and 24 h without stirring were necessary. The conjugates were purified by RP-HPLC on a preparative C8 column using a linear acetonitrile or methanol (0.1% TFA) gradient in an aqueous solution (0.1% TFA). Peptides were purified by analytical RP-HPLC using a C8 column with a linear acetonitrile or methanol (0.1% TFA) gradient in an aqueous solution (0.1% TFA) and characterized by MALDI-TOF MS.

2.2. Internalization of the conjugates

2.2.1. Cell Culture [4]

Wild type (CHO-K1) and xylose transferase deficient (pgsA745) Chinese hamster ovary cells were obtained from the American Type Culture Collection (Manassas, VA). All cell lines were grown under an atmosphere of 5% CO_2 in air and 100% relative humidity in F12 growth medium (DMEM) supplemented with 10% (v/v) fetal bovine serum, 100 μg/mL of streptomycin sulfate, amphotericin B, and 100 units/mL of penicillin G.

2.2.2. Measure of the cellular uptake by MALDI-TOF mass spectrometry

The internalization experiments were performed as described previously [18,19]. The conjugates contain an isotope tag (Biot(O_2)-GGGG), located on the N terminus of the cargo of the PKCi peptide (Table 1 and Fig. 1) to allow absolute quantification by MALDI-TOF MS. Two PKCi peptide analogs were synthesized, one with four non-deuterated glycines (^{1}H-peptide) and one with four deuterated glycines (^{2}H-peptide). One million adherent cells were incubated at 37 °C for 75 min with the conjugate ^{1}H-peptide (5 μM) in culture medium (without fetal calf serum). After washing with culture medium, cells were treated with a TCEP solution for 3 min (2 mM TCEP in 50 mM Tris, pH 7.5) to reduce the PKCi species linked by a disulfide bridge to cell surface thiols [24,25]. Trypsin was then added to degrade the remaining extracellular and membrane-bound peptide and to detach cells. After addition of enzyme inhibitors mixed with bovine serum albumin, cells were transferred to a microtube, centrifuged, and washed with Tris buffer. The cells were then lysed in a solution containing a controlled and relevant quantity of the chemically

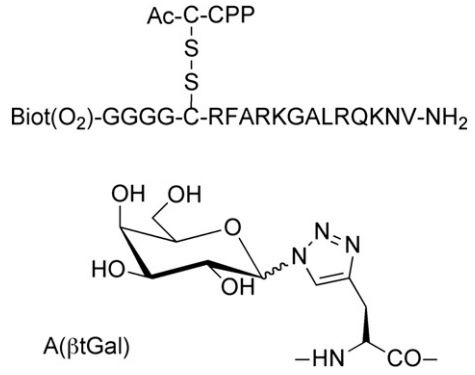

Fig. 1. General formula of PKCi-CPP disulfide conjugates (**1′**) to (**5′**), with CPP sequence indicated in italic in Table 1, and formula of the alanyl-modified residue: A(βtGal).

identical deuterated form (^{2}H) of the PKCi (which served as internal standard to quantify by MALDI-TOF the internalized amount of ^{1}H-CPP). The sample was then boiled for 15 min to inhibit intracellular protease activity and to destroy potential PKCi intracellular partners molecular interactions. The biotinylated PKCi analogs (^{1}H and ^{2}H) were then purified with streptavidin-coated magnetic beads and eluted with the α-cyano-4-hydroxy cinnamic acid matrix before MALDI-TOF MS analysis. The amount of intact internalized PKCi was calculated from the area ratio of the $[M+H^+]$ signals of intact ^{1}H-peptide and ^{2}H-peptide. The ^{1}H- and ^{2}H-peptides are separated by 8 atomic mass units, so there was no overlap of their signals on the mass spectra. As for standard quantity, we found quantification to be more accurate when the ^{1}H-PKCi/^{2}H-PKCi signals ratio ranged from 0.2 to 5. In addition, for each experiment, we used duplicate or triplicate wells, and the experiments were independently repeated for at least three times, as indicated in the figures. The minimal amount, which can be confidently determined, was around 0.5 pmol of intact peptide, corresponding to intracellular concentrations around 0.5 μM (mean volume of 1 pl per CHO cell). The trypsinization step was omitted for the determination of the membrane-bound peptide. Mix 4 (ou Proteomix): [500–3500 Da] was used for peptide calibration.

2.3. Biophysical studies

2.3.1. Preparation of MLVs and LUVs

Lipid films were made by dissolving the appropriate amount of lipids into $CHCl_3$ or a mixture of $CHCl_3$ and CH_3OH (2/1, vol/vol). The solvent was then evaporated under N_2 to deposit the lipid as a film on the wall of a test tube. Final traces of solvent were removed in a vacuum chamber attached to a liquid nitrogen trap during 3–4 h. Films were then hydrated with 10 mM Tris, 0.1 M NaCl, 2 mM EDTA, pH 7.5 for DSC and ITC experiments. The films were then vortexed extensively at a temperature superior to the phase transition temperature of the lipid to obtain MLVs. To form LUVs, the MLVs were subjected to five freeze/thawing cycles. The homogeneous lipid suspension was passed 10 times through a nitrogen pressure driven extruder (LIPEX, Northern Lipids Inc., BC) equipped with a 100 nm polycarbonate membrane at a temperature above the phase transition temperature of the lipid.

2.3.2. Differential scanning calorimetry (DSC) experiments

DSC experiments were performed on a high-sensitivity calorimeter (TA Instruments). The different peptides were gradually added to the same sample of lipid MLVs to obtain peptide/lipid molar ratios of 1/100, 1/50, 1/25 and 1/10. The lipid concentration was 1 mg/mL, ca. 1.45 mM. For each peptide concentration, a minimum of four heating and four cooling scans were performed so that equilibrium is reached. A scan rate of 1 °C/min was used and there was a delay of 10 min between sequential scans in a series to allow thermal equilibration. Data analysis was performed by the fitting program NanoAnalyze provided by TA Instruments.

2.3.3. Isothermal titration calorimetry (ITC) experiments

ITC experiments were performed on a TA Instrument nano ITC calorimeter. To avoid air bubbles, peptide and LUV solutions were degassed under vacuum before use. Titrations were performed by injecting aliquots of LUVs (lipid concentration varying between 6.24 mM and 3.12 mM) into the calorimeter cell containing the peptide solution (peptide concentration 0.1 mM except for (**5**) 0.048 mM), with 5 min waiting between injections. The experiments were performed at 25 °C. Data analysis was performed using the program NanoAnalyze provided by TA Instruments.

2.3.4. Surface pressure measurements and Imaging Ellipsometry

Monolayer experiments were performed in a Teflon circular Langmuir trough (V = 12 mL, ø = 6.5 cm). The surface pressure was measured using the Wilhelmly method using a filter paper plate. All the experiments were performed at 27 ± 2 °C. The trough was filled with 20 mM Tris, 150 mM NaCl buffer, pH 7.5. Monolayers were obtained by depositing few μL of a lipid mixture (DMPC in $CHCl_3$ or DMPC/DMPG 80/20 in $CHCl_3/CH_3OH$, 2/1) at the air/buffer interface until the surface pressure reached a value between 25 and 28 mN/m. Fifteen microliters of each peptide in solution (1 mM) in the same buffer was then injected under the monolayer into the subphase as three successive injections and the surface pressure was monitored continuously. At the same time, the morphology of the interface was observed using an Imaging Ellipsometer (NFT iElli-2000) mounted on the Langmuir trough. The microscope was equipped with a frequency-doubled Nd:Yag laser (532 nm, 55 mW), a polarizer, an analyzer and a CCD camera. The spatial resolution of the BAM was ~2 μm and the image size 570 × 450 μm with 10× lens used.

2.3.5. ATR spectra of the peptides in solution or in the presence of phospholipid multibilayers

The ATR spectra of the peptide in solution were recorded on a Nicolet 6700 spectrometer. For the spectra of the peptides alone in solution, the spectrometer was equipped with a 3 reflexion diamond crystal. The peptides were dissolved in a 20 mM Tris, 150 mM NaCl buffer, pH 7.5. Eight hundred scans were acquired at a resolution of 8 cm^{-1}. The experiments were performed at room temperature.

For the spectra of the peptides in the presence of multibilayers, the spectrometer was equipped with a Germanium crystal thermostated at 30 °C. ATR spectroscopy is sensitive to orientation and therefore spectra were recorded with a parallel (*p*) or perpendicular (*s*) polarization of the incident light with respect of the ATR plate. 800 scans were coadded at a resolution of 8 cm^{-1}. The multibilayer system was formed by depositing 30 μL of a solution of DMPC/DMPG (80/20) in $CHCl_3/CH_3OH$, 2/1 (lipid concentration 0.5 mg/mL) on the surface of the crystal and the solvents are left to evaporate. A *p* and an *s* spectrum are recorded to confirm that the system is well oriented and that no traces of chloroform are left. The system is the re-hydrated by adding 20 μL of 20 mM Tris, 150 mM NaCl, pH 7.5 buffer. One to 2 μL of peptide solution (1 mM) in the same buffer is added, leading to a final peptide concentration of 50 μM to 100 μM, and *p* and *s* spectra are recorded. The amide I frequencies were attributed as follow: <1630 cm^{-1} antiparallel beta sheet, 1630–1635 cm^{-1} parallel beta sheet, 1640–1650 cm^{-1} random coil, 1650–1662 cm^{-1} alpha helix, 1662–1680 cm^{-1} beta turn.

3. Results and discussion

All the peptides and their conjugates (Table 1, Fig. 1) were prepared by Fmoc solid phase peptide synthesis. The galactosyl moieties were introduced on a Pra-containing precursor (Fig. 2), as we recently reported [13]. All CPPs and conjugates were obtained with purity above 95%, even though in some cases yields were sacrificed to ensure a better purity, and characterized by MALDI-TOF mass spectrometry (Table 2, Fig. 3A).

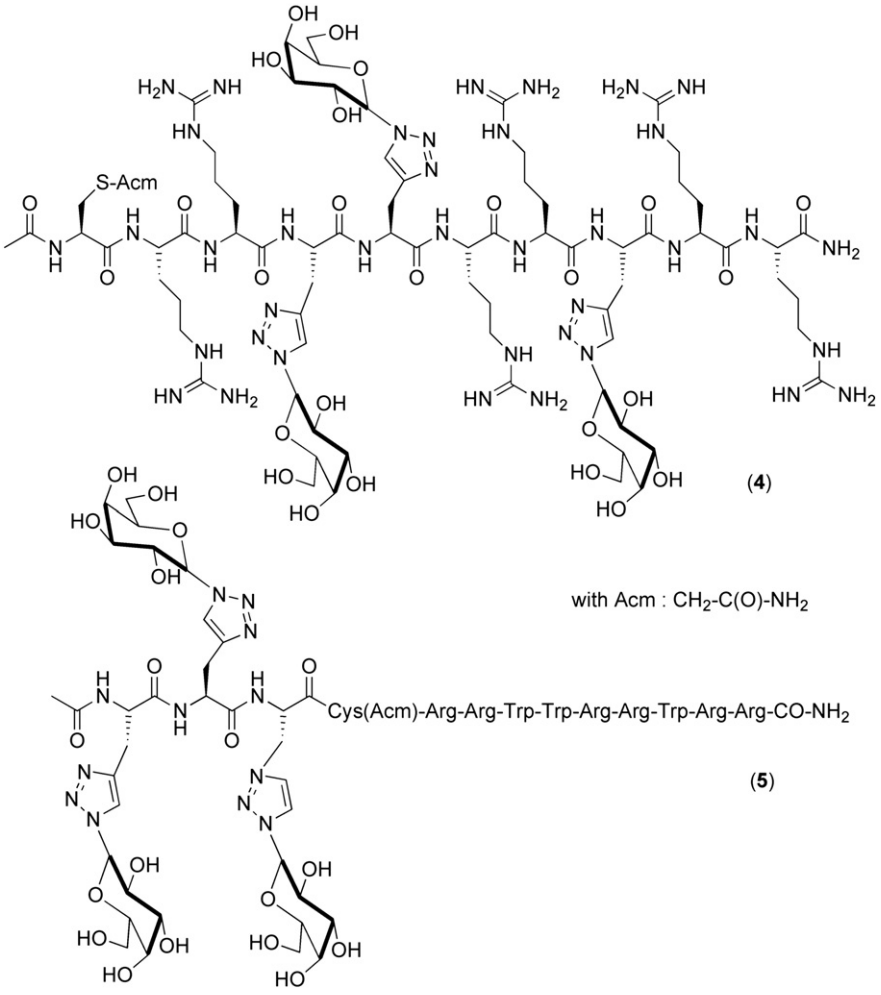

Fig. 2. Formula of peptides (**4**) and (**5**), as examples of galactosyl-linked triazole CPPs.

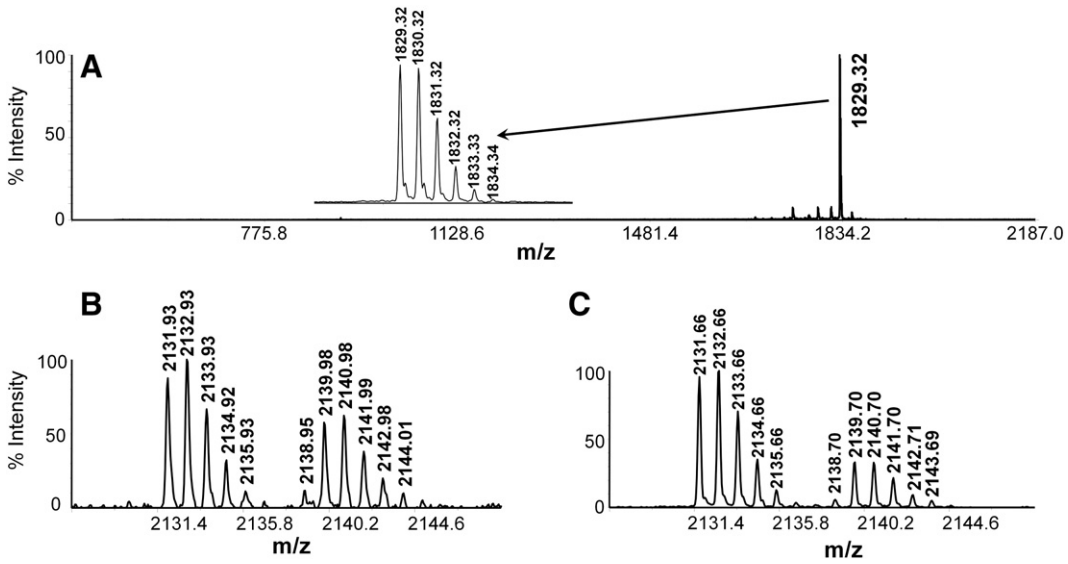

Fig. 3. Examples of MALDI-TOF MS spectra. **A**) Peptide (**3**). **B**) Quantification of membrane bound conjugate (**1′**). After treatment without the incubation step with trypsin (Cf. Material and methods), the PKCi-SH peptide, Biot(O_2)GGGGCRFARKGALRQKNV-NH_2, was recovered after cells lysis in a solution containing a controlled and relevant quantity (here: 100 pmol) of the chemically identical deuterated form of the ^{2}H-PKCi-SH peptide (Biot(O_2)-[^{2}H]G-[^{2}H]G-[^{2}H]G-[^{2}H]G-C-RFARKGALRQKNV-NH_2), which served as an internal standard to quantify the amount of ^{1}H-CPP. The amount of the intact membrane bound plus the internalized PKCi was calculated from the area ratio of the [M,H$^+$] signals of intact ^{1}H-PKCi-SH and ^{2}H-PKCi-SH (found: 274 pmol). **C**) Quantification of internalized PKCi with conjugate (**5′**). After treatment with the incubation step with trypsin (Cf. Material and methods) the PKCi-SH peptide was recovered after cells lysis in a solution containing the [^{2}H]-PKCi-SH peptide (here: 2 pmol). The amount of intact internalized PKCi was calculated from the area ratio of the [M,H$^+$] signals of intact ^{1}H-PKCi-SH and ^{2}H-PKCi-SH (found: 3.2 pmol).

3.1. Quantification of membrane-bound and internalized PKCi peptides with wild type CHO (CHO-K1) and GAG-deficient CHO (CHO-pgsA-745) cells

The PKCi cargo was used to quantify the efficiency of delivery of our different carriers and not the KLAK cargo studied previously [13] because this peptide is prone to aggregation. In addition the KLAK peptide is not sensitive to the treatments used to distinguish the internalized species from the membrane-bound species by MALDI-TOF [18,19,24,25]. These two cargoes allowed us to study the cell uptake of the different CPPs by two complementary strategies: PKCi permitted a direct quantification of the internalized cargo, whereas using KLAK we showed that the studied CPPs could transport a bioactive cargo and that a biological response could be observed with different efficiencies according to the vector [13]. All the CPPs (**1**–**5**) and conjugates (**1′**–**5′**) have the same *N*-terminus modifications. The only difference within the sequence of CPPs (**1**–**4**) corresponds to the gradual replacement of the tryptophan(s), and thus the indole side-chain(s), by galactosyl moiety(ies). CPP (**5**) has three tryptophans in the sequence and three galactosyl residues on the N-terminus.

3.1.1. Quantification of membrane-bound conjugates (**1′**–**5′**)

Conjugates (**1′**–**5′**) were incubated, at 5 μM, for 75 min with both CHO cell types (10^6 cells). Cells were first washed with culture medium, then after cell lysis the amount of peptide was quantified by MALDI-TOF, which corresponds to both the conjugate bound to the cell membrane and internalized inside the cells. An example of this quantification is shown on Fig. 3B. The amount of conjugate bound to the CHO-K1 cells ranged from 60 to 110 pmol, and similar data were obtained with CHO pgsA-745 cells (60 to 70 pmol, whatever the conjugate) (Fig. 4A).

These membrane-bound species correspond to peptides inserted into the lipid bilayer or covalently linked to cell surface thiols [24,25] or associated to high-affinity binding sites in the membrane, such as sialic acid and/or lipids present on both wild type and GAG-deficient CHO cells. As previously quoted for CPPs alone, there is no direct relationship between the amount of high-affinity membrane-bound peptide and the internalized quantity [4,18,19].

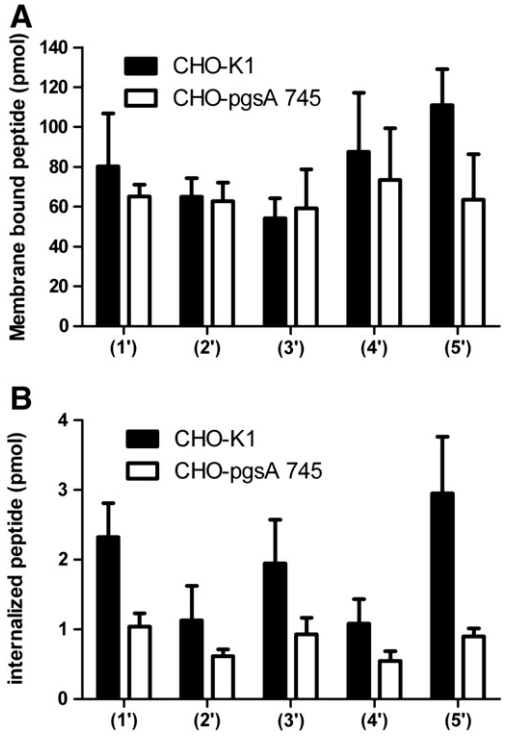

Fig. 4. Quantification of membrane-bound (**A**) and internalized (**B**) peptides for conjugates (**1′**) to (**5′**) using wild type CHO cells (black bars) and GAG-deficient CHO cells (white bars). Incubation conditions: 5 μM of conjugate with 10^6 cells at 37 °C for 75 min. The error bars represent the standard deviation (SD).

3.1.2. Cargo internalization via conjugates (**1′**–**5′**)

The amount of internalized cargo was measured after removing the membrane-bound conjugates by TCEP treatment followed by trypsin digestion. In both cell types, the amount of internalized cargo, Biot-(O_2)-GGGG-C-PKCi, represented 1 to 2.5% of the membrane-bound conjugate. PKCi was internalized more efficiently into CHO-K1 cells (1.1 to 3.1 pmol) than into GAG-deficient CHO cells. An example of this quantification is shown in Fig. 3C. The most potent vector with CHO-K1 cells were peptides (**1′**), (**3′**) and (**5′**), which led to the internalization of 2.3, 2 and 3.1 pmol of PKCi, respectively, these peptides being 2- to 3-times more efficient than peptides (**2′**) and (**4′**) (Fig. 4B). The amount of PKCi internalized into CHO-pgsA-745 cells ranged from 0.5 to 1 pmol, with the following rank of potency: (**2′**) = (**4′**) < (**1′**) = (**3′**) = (**5′**).

Comparison of the efficiency of these conjugates showed that in both cell lines the Trp residues (indole side-chain) in the CPP sequence are crucial for the cargo to be internalized, Ala and Ala-substituted galactosyl residues drastically reduce the internalization. Conjugate (**5′**) with three galactosyl units on the *N*-terminus but with three tryptophans enters efficiently CHO cells. Conjugate (**2′**) with three alanines is less efficient than (**1′**) in entering CHO cells, in contrast to previously reported for Jurkat cells [14]. Globally, the internalization results we report herein are consistent with the biological activity we had previously observed when the CPPs were conjugated to the pro-apoptotic KLAK peptide [13]. When conjugated to the CPPs containing three and two Trp residues, the incubation of KLAK induced CHO-K1 cell death whereas no effect on cell viability was observed when KLAK was conjugated to the peptide containing three galactosyl moieties instead of tryptophans.

3.2. Probing the effect of the vector peptides (**1**–**5**) on DMPG lipid phase transition by DSC

The interaction of peptides (**1**–**5**) with phospholipids was studied by monitoring the way these peptides affect the L_{β}' gel phase to the P_{β}' ripple phase (pre-transition T_{pre}) and the P_{β}' ripple phase to the L_{α} fluid phase (main transition, T_m) transitions of DMPG (thermograms on Fig. 5). Although anionic lipids are not major constituents in the external leaflet of eukaryotic cells, they are present and their role becomes important when they get concentrated in larger membrane areas, a process induced by other membrane active peptides [26,27]. This aspect together with our previous observations on the importance of electrostatic interactions between the peptide Arg_6/Trp_3, an analog of peptide (**1**), and the lipids [28] led us to make this lipid choice.

All the peptides affect the pre-transition, which was completely abolished at the highest peptide concentrations. The thermograms corresponding to P/L = 1/10 are presented but, at this peptide concentration a high turbidity is often observed, corresponding to phenomena such as vesicle fusion and/or precipitation. In the case of the main transition, different behaviors could be observed depending on the peptides. Peptides (**2**) and (**4**) did not induce significant perturbation on the main transition of DMPG, and no shift of T_m were observed. The enthalpy of the main transition only slightly increased, due to little broadening of the peak. On the other hand, the main transition of DMPG was strongly affected by the addition of (**1**), (**3**) and (**5**): the addition of peptide induced a shift of T_m to lower temperatures, this shift being especially intense in the case of (**1**) and (**5**). This decrease in T_m (Table 3) indicates that these three peptides interact more favorably with the fluid than the gel phase or in other terms that these peptides have a fluidizing effect on the model bilayer.

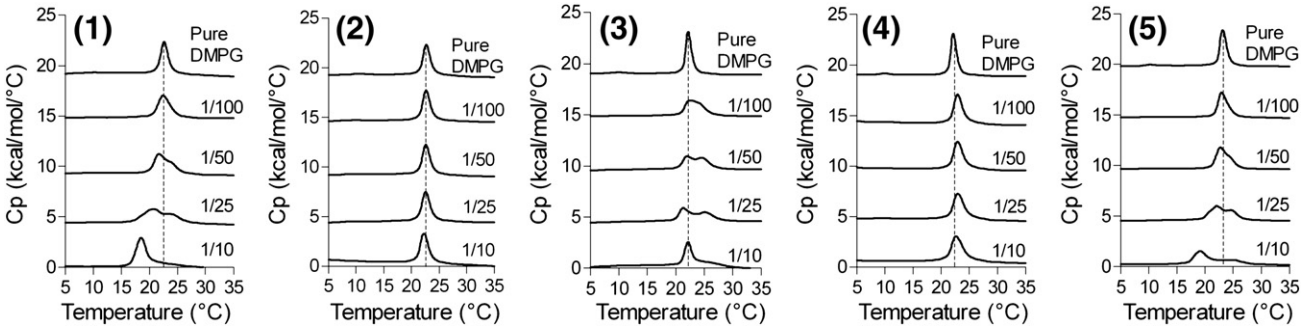

Fig. 5. DSC thermograms illustrating the effect of the addition of peptides (**1**) to (**5**) to DMPG MLVs (1 mg/mL). The curves correspond to pure lipid and peptide to lipid ratios of 1/100, 1/50, 1/25 and 1/10.

Peptides (**1**), (**3**) and (**5**) also affected the enthalpy of transition ΔH_m (Table 3) and induced an important broadening and flattening of the main transition peak. A change in ΔH_m is the consequence of the disruption of van der Waals interactions between the hydrocarbon chains. It shows that the three peptides were able to intercalate between the fatty acid chains. Finally, addition of peptides (**1**), (**3**) and (**5**) induced the splitting of the main transition peak, which has been suggested in the literature to arise from the coexistence of peptide-rich and peptide-poor domains in the bilayer [29–31].

DSC studies with DMPG provided information on the mode of interaction with lipids both in the gel and fluid phases and the way they perturb the phase transition between these two states. For all peptides investigated, the disappearance of the pre-transition arising from the tilting of the hydrocarbon chains, suggests electrostatic interactions between the cationic peptides (**1**–**5**) and the negatively charged headgroups of DMPG. Peptides (**1**), (**3**) and (**5**) modify the main transition involving the lipid chains, whereas peptides (**2**) and (**4**) do not affect it at all, suggesting a rather superficial contact between these two peptides and the lipid headgroups. The modification of lipid fluidity by peptides (**1**), (**3**) and (**5**) may reflect their capacity to intercalate between the fatty acid lipid chains. For these three peptides, increasing the peptide concentrations induces the splitting of the main transition peak, the difference in the T_m values of the two peaks increases with concentration of peptides (**1**), (**3**) and (**5**), without strongly affecting the area/population of the two corresponding states. These two peaks can be assigned to different modes of peptide association, as the DSC experiments were performed with pure DMPG. The weak differences in the T_m values between these two states exclude the existence of morphological equilibrium between micelles, lamellar and hexagonal phases. In the lamellar phases, the correlation time for lateral diffusion is greater than 10^{-5} s and the formation of supramolecular assemblages occurs starting from very small rafts (diameter <10 nm) to larger ones (from 30 to 230 nm) in timescales in the range of 10^{-3} s [34,35]. Thus, within the experiment time (several minutes for each scan), the lateral diffusion of lipids and/or the formation of assemblages can readily occur leading to homogeneous peptide distribution on the membrane surface.

Table 3
Thermodynamic parameters obtained by DSC for pure DMPG and DMPG interacting with peptides (**1**) to (**5**) at a peptide to lipid ratio of 1/25. T′ represents the second peak maximum if a peak splitting is observed.

	T_{pre} (°C)	ΔH_{pre} (kcal/mol)	T_m (°C)	ΔH_m (kcal/mol)	T′ (°C)
Pure DMPG	10.3	0.18	22.8	5.72	–
(**1**)	–	–	20.8	7.8	24.3
(**2**)	–	–	22.6	6.3	–
(**3**)	–	–	21.2	6	25.1
(**4**)	9.7	0.06	22.9	6.5	–
(**5**)	–	–	22.1	6.1	24.8

Three different hypotheses may be evoked to explain the slow exchange rate between the two states observed in the DSC experiments for peptides (**1**), (**3**) and (**5**), all originating from a nonhomogenous distribution of the CPP on the lipid surfaces. Firstly, an equilibrium between monomeric versus aggregated forms of the CPP on the surfaces of all MLVs bilayers may lead to the formation of "peptide-rich" and "peptide-poor" domains, which may be achieved by an accumulation of the CPP, provided the micromolar affinity of the studied peptides for negatively charged bilayers. Secondly, the presence of the CPPs on both the external bilayer and inside ones, which perturb/interact distinctly with the different curvatures of different lipid layers leading also to the splitting of the transition peak. Thirdly, the CPP may interact with MLVs of different sizes, the peptides may indeed induce the formation of smaller liposomes or micelles with different curvatures, this is quite common for peptides possessing even moderate "detergent activity" [36–39]. During the DSC experiment, a total of eight heating and cooling scans at 1 °C/min are performed, therefore the peptides are interacting with the lipids in the gel and fluid phase or at the phase transition for long periods of time. Our hypothesis is that during the runs, peptides (**1**), (**3**) and (**5**) are able to translocate through the bilayer and therefore equilibrate between the different layers of the MLVs, although the amounts of peptide in the external layer and internal ones might be different. The different peptide distribution among the different MLV layers can explain the splitting observed in the thermogram, but no lipid layer of the MLVs remains unexposed to peptide as no T_m signal at a value corresponding to pure DMPG is ever observed for peptides (**1**), (**3**) and (**5**). When the main transition peak is not affected or split, the peptide may remain only superficially attached to the bilayer. In this study, CPP (**2**) and (**4**) internalized poorly into CHO cells and they do not induce any change in the T_m, as we have already observed for Arg_6/Leu_3 [28]. Arg_9, which is an efficient CPP, did not affect the T_m value of DMPG MLVs, though a broadening of the transition peak could be observed [28]. Arg_9 probably presented a homogenous distribution on all the lipid bilayers of DMPG MLVs, which is not the case for the CPPs (**1**), (**3**) and (**5**). In the present work, it is difficult to distinguish between homogeneous peptide distribution due to peptide aggregation and distinct translocation processes through the MLVs with or without fragmentation of the MLVs or concomitant phenomena.

3.3. Binding of the peptides to DSPG LUVs probed by ITC

The interaction of peptides (**1**–**5**) with phospholipids was also studied using ITC (Table 4, Fig. 6). Aliquots of LUVs composed of pure DSPG were injected into the calorimeter cell containing the peptide solution. The anionic lipid DSPG was used instead of DMPG because we have previously observed that the interaction of CPPs with DMPG often leads to quite complex binding curves, probably due to the higher capacity of this lipid to reorganize in different supramolecular assemblages. From

Table 4
Thermodynamic parameters of peptides binding to DSPG LUVs determined by ITC at 25 °C.

Peptides	K_A (M^{-1})	K_D (μM)	ΔH (kJ/mol)	ΔG (kJ/mol)	ΔS (kJ/mol/K)	n
(**1**)	12.5 10^5	0.80	−3.07	−44.7	0.140	5.7
(**2**)	2.53 10^5	3.96	−1.70	−40.8	0.131	3.8
(**3**)	9.50 10^5	1.05	−2.00	−44.1	0.141	4.2
(**4**)	1.02 10^5	9.80	−1.09	−38.5	0.126	6.2
(**5**)	2.17 10^5	4.6	−2.28	−40.4	0.128	4.9

the experiments, different parameters can be derived: i) the binding enthalpy of the peptide to the liposome (ΔH), ii) an apparent K_A representing the affinity of the peptide for the liposome and iii) the stoichiometry of binding n, i.e. the number of phospholipid per peptide. The dissociation constant K_D, the Gibbs free enthalpy (ΔG) and the entropy (ΔS) of binding were derived from the K_A and ΔH. The binding isotherms are displayed in Fig. 6 and the derived thermodynamic data are given in Table 4. For all the peptides, binding to DSPG LUVs was an exothermic process, and therefore enthalpy driven. Peptide (**1**) had the strongest affinity for the liposomes followed by (**3**). The affinity of (**2**) was intermediate and peptides (**4**) and (**5**) had weaker affinities. Peptide (**4**) had more than ten times less affinity for the DSPG LUVs compared to (**1**). The lowest ΔH corresponds to (**1**) and (**5**) (both with three Trp) whereas the highest ΔH correspond to (**2**) and (**4**) (no Trp), peptide (**3**) (with two Trp) has intermediate ΔH. The stoichiometry of binding varied between 4 and 6, being around the number of guanidinium side-chains for the peptide.

The interactions of CPPs (**1**), (**3**) and (**5**) led to more favorable enthalpy when compared with peptides (**2**) and (**4**), and there is a quite good correlation between the number of Trp residues in the peptide and the enthalpy (favorable) associated with peptide/lipid interaction. The energetically favorable transfer of Trp residues from an aqueous to a hydrophobic environment (membrane core) can explain the increase in enthalpy with the number of Trp residues. Most interesting to quote is that such favorable enthalpy seems to affect the peptides' capacity to enter cells. Indeed, there is a certain relationship between the enthalpy and the CPP internalization efficiency in CHO cells. Thus, the favorable enthalpy associated with Trp transfer into the lipid membrane may be the prominent driving force among others to insert into the membrane and induce the necessary lipid bilayer perturbation for cellular internalization.

3.4. Peptide insertion in monolayers and interface morphology

The insertion of the peptides in monolayers composed of pure DMPC or DMPC/DMPG (80/20) was studied by following the surface pressure at the air/buffer interface in a Langmuir trough using the Whilelmy method. The monolayer thickness was evaluated to be around 13 Å. None of the peptides induced any change in the surface pressure when injected underneath a DMPC monolayer. Different behaviors were observed when the peptides where injected beneath the DMPC/DMPG monolayers. Comparison of the peptides (**1** to **5**) showed that only peptides (**1**) and (**5**) induced an increase (0.3 mN/m to 0.6 mN/m per injection) in surface pressure, showing that they were able to slightly insert into the DMPC/DMPG monolayer (data not shown). However, these variations remained weak compared to the strong increase in the surface pressure we previously reported [40] for Substance P, a primary amphipathic neuropeptide, or as reported for other CPPs [41]. The SP backbone was shown to penetrate into the lipidic layer, suggesting that in the case of CPPs (**1**) and (**5**) only a limited insertion of the tryptophan side chains into the lipid layer should occur. For penetratin it has been proposed that its two tryptophans, orientated parallel to the membrane, anchor the peptide on the surface [42–44]. In membrane mimetic environments penetratin is more or less helical with its axis parallel to the membrane surface, as previously reported [32] and further confirmed by polarized-light spectroscopy [45].

At the same time, the morphology of the interface was monitored using Imaging Ellipsometry. After injection of the different peptides, domains corresponding to different gray level intensities on the image (Fig. 7) appeared. The domains were comparable for every peptide with very irregular shapes and growing in size along time. In some cases for peptides (**1**), (**2**) and (**3**), the thickness of the domain could be evaluated from their reflection intensity around 35 Å. Such domains may be related with the more favorable interaction and subsequent recruitment of anionic lipids by the peptide as already observed by DSC studies [26,27].

3.5. Peptide structure determined by ATR spectroscopy

ATR spectroscopy allowed studying the structure of the peptides in solution as well as in the presence of model phospholipid membranes. In solution, after the subtraction of the buffer absorption, the amide I band was well defined at 1643 cm^{-1}, showing that all the peptides were mainly random in buffer. In the presence of multi-bilayers deposited on the ATR crystal, a shift in position for the amide bands was observed (Table 5). Peptides (**2**) and (**5**) had well defined amide I bands at 1658 cm^{-1} and 1657 cm^{-1}, respectively for both *p* and *s* polarizations, showing that these two peptides have a helical structure in contact with the model membrane. For peptides (**1**), (**3**) and (**4**), the situation was less clear. For *p* polarization, the amide I bands are all located around 1652 cm^{-1}, showing helical content. However for *s* polarization, the position of the amide I bands corresponds to a random coil. Therefore, there is

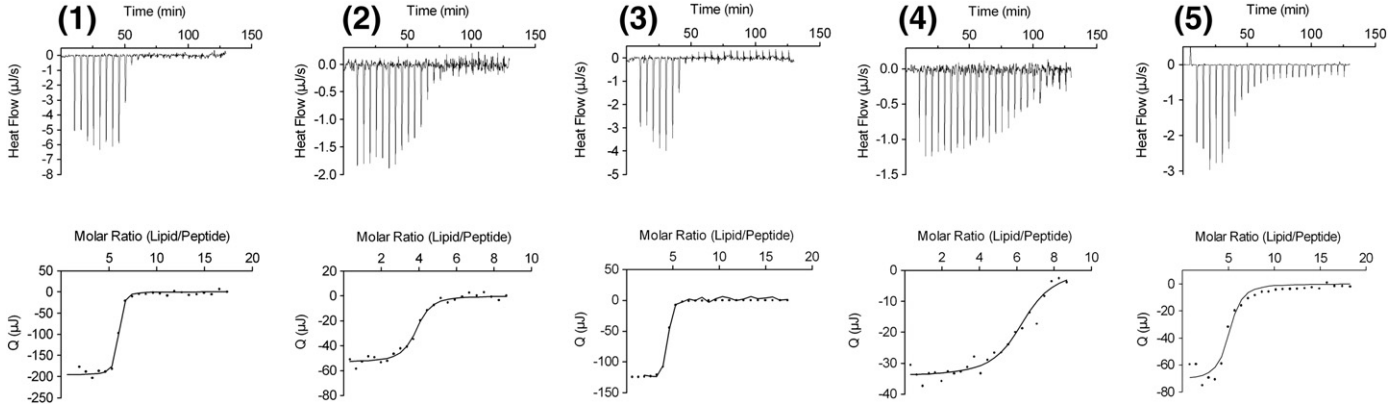

Fig. 6. Isothermal titration of DSPG LUVs (6.24 mM or 3.12 mM) into peptides (**1**) to (**5**) (peptide concentration 100 μM, except (**5**) 48 μM) at 25 °C. The lower curves represent the heat of reaction measured by peak integration as a function of lipid/peptide ratio. The solid lines represent the best fit to experimental data. The thermodynamic parameters are summarized in Table 4.

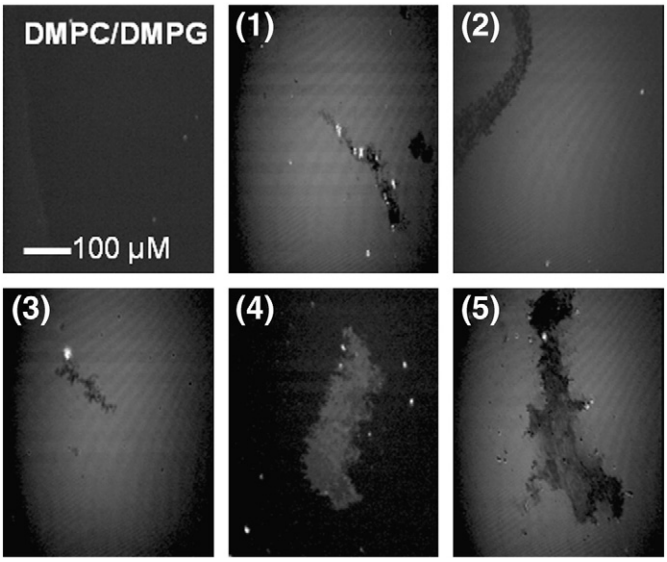

Fig. 7. Ellipsometry images of a DMPC/DMPG (80/20) monolayer at a water–air interface and after injection of peptides (**1**) to (**5**) in the subphase. The monolayer appears in gray and domains in dark, except for peptide (**4**) where the monolayer appears in dark and the domain in gray.

probably a mixture of structures for these peptides, with helices probably more oriented along the *z* axis bilayer and the random coil without specific orientation. The accumulation of peptides (**1**–**5**) in the membrane shifted the random coil conformations observed in solution towards helical structures as revealed by ATR spectroscopy. Thus, these five CPP (**1**–**5**) accumulate on the surface, lying probably parallel to the membrane according to their secondary amphipathic structure, and depending on the presence of the tryptophan sidechains a subsequent insertion of the indoles may allow the transfer of the CPP and its cargo into the lipid bilayer.

4. Conclusion

With the series of CPPs studied here we have shown that tryptophan residues play a key role in the insertion of a CPP and its conjugate in the membrane, and that galactosyl residues hamper the internalization when introduced in the middle of the amphipathic secondary structure of a CPP but not on the *C*-ter, as long as tryptophan residues are still present in the sequence. The insertion of these CPPs into membrane models is enthalpy driven and correlates with the number of tryptophans in the sequence of these secondary amphipathic CPPs. Reported NMR studies by our laboratory on an analog of Arg_6/Trp_3 have indicated the existence of π-cation interactions between the Trp and Arg residues of this CPP [32]. Tryptophan residues via the π-cation interaction may promote/allow the crossing of the lipidic membrane core by the cationic peptide (or peptide rich in cationic residues), a process that would be highly unfavorable otherwise. Such contact not being possible in the case of peptide Arg_6/Ala_3, and in the case of Arg_6/Leu_3 peptide [28], both peptides fail to enter cells. Deshayes et al. have also proposed that tryptophans are important in the function of their lead CPP (CADY), even though "the reasons of their importance are unclear" [33]. Chan et al. have highlighted the crucial chemical properties of Arg and Trp residues in antimicrobial peptides. They proposed that Trp should have a distinct preference for the interfacial region of lipid bilayers, while Arg residues allow adequate interactions with the anionic components of bacterial membranes [46].

We have observed with DMPG MLVs that some peptides, which are efficient CPPs, lead to T_m splitting, suggesting that during the DSC experiments these CPPs may distribute non-homogeneously in the lipids, a process due to either the peptide internalization into the internal MLVs bilayers at different levels and/or peptide auto-association. Peak splitting in the main lipid phase transition may help identifying efficient CPPs. However, this might not be a prerequisite, as efficient CPPs may not induce a T_m splitting, depending probably on the overall distribution of the CPP within the MLV bilayers, and/or their propensity to auto-associate. The CPPs investigated herein present a certain propensity to aggregate in contact with the lipid surface, whether this property is related to the observed differences in terms of uptake needs further studies.

Table 5
Amide I band position on ATR spectra for *p* and *s* polarizations for peptides (**1**) to (**5**) in contact with multi-bilayers composed of DMPC/DMPG (80/20) supported on the ATR crystal and the associated probable secondary structure.

	Amide I band position (cm^{-1}) (*p*/*s* polarization)	Probable structure
(**1**)	1652/1639	α-Helix/Random Coil
(**2**)	1658/1658	α-Helix
(**3**)	1653/1641	α-Helix/Random Coil
(**4**)	1652/1646	α-Helix/Random Coil
(**5**)	1657/1657	α-Helix

Acknowledgements

The authors wish to thank Rodrigue Marquant for the synthesis of the PKCi peptide.

References

[1] F. Duchardt, M. Fotin-Mleczek, H. Schwarz, R. Fischer, R. Brock, A comprehensive model for the cellular uptake of cationic cell-penetrating peptides, Traffic 8 (2007) 848–866.
[2] P. Lundin, H. Johansson, P. Guterstam, T. Holm, M. Hansen, U. Langel, S. El Andaloussi, Distinct uptake routes of cell-penetrating peptide conjugates, Bioconjug. Chem. 19 (2008) 2535–2542.
[3] E. Vives, J. Schmidt, A. Pelegrin, Cell-penetrating and cell-targeting peptides in drug delivery, Biochim. Biophys. Acta 1786 (2008) 126–138.
[4] C.Y. Jiao, D. Delaroche, F. Burlina, I.D. Alves, G. Chassaing, S. Sagan, Translocation and endocytosis for cell-penetrating peptide internalization, J. Biol. Chem. 284 (2009) 33957–33965.
[5] C.L. Watkins, D. Schmaljohann, S. Futaki, A.T. Jones, Low concentration thresholds of plasma membranes for rapid energy-independent translocation of a cell-penetrating peptide, Biochem. J. 420 (2009) 179–189.
[6] A. Thomas, L. Lins, G. Divita, R. Brasseur, Realistic modeling approaches of structure–function properties of CPPs in non-covalent complexes, Biochim. Biophys. Acta 1798 (2010) 2217–2222.
[7] B. Aussedat, S. Sagan, G. Chassaing, G. Bolbach, F. Burlina, Quantification of the efficiency of cargo delivery by peptidic and pseudo-peptidic Trojan carriers using MALDI-TOF mass spectrometry, Biochim. Biophys. Acta 1758 (2006) 375–383.
[8] B. Aussedat, E. Dupont, S. Sagan, A. Joliot, S. Lavielle, G. Chassaing, F. Burlina, Modifications in the chemical structure of Trojan carriers: impact on cargo delivery, Chem. Commun. (2008) 1398–1400.
[9] D. Delaroche, B. Aussedat, S. Aubry, G. Chassaing, F. Burlina, G. Clodic, G. Bolbach, S. Lavielle, S. Sagan, Tracking a new cell-penetrating (W/R) nonapeptide, through an enzyme-stable mass spectrometry reporter tag, Anal. Chem. 79 (2007) 1932–1938.
[10] S. Lavielle, N.C. Ling, R.C. Guillemin, Solid-phase synthesis of two glycopeptides containing the amino acid sequence 5 to 9 of somatostatin, Carbohydr. Res. 89 (1981) 221–228.
[11] R. Polt, F. Porreca, L.Z. Szabo, E.J. Bilsky, P. Davis, T.J. Abbruscato, T.P. Davis, R. Harvath, H.I. Yamamura, V.J. Hruby, Glycopeptide enkephalin analogues produce analgesia in mice: evidence for penetration of the blood–brain barrier, Proc. Natl. Acad. Sci. U.S.A. 91 (1994) 7114–7118.
[12] K. Michael, V. Wittmann, W. Konig, J. Sandow, H. Kessler, S- and C-glycopeptide derivatives of an LH-RH agonist, Int. J. Pept. Protein Res. 48 (1996) 59–70.
[13] L. Dutot, P. Lecorche, F. Burlina, R. Marquant, V. Point, S. Sagan, G. Chassaing, J.M. Mallet, S. Lavielle, Glycosylated cell-penetrating peptides and their conjugates to a proapoptotic peptide: preparation by click chemistry and cell viability studies, J. Chem. Biol. 3 (2009) 51–65.
[14] J.B. Rothbard, E. Kreider, C.L. VanDeusen, L. Wright, B.L. Wylie, P.A. Wender, Arginine-rich molecular transporters for drug delivery: role of backbone spacing in cellular uptake, J. Med. Chem. 45 (2002) 3612–3618.
[15] C. House, B.E. Kemp, Protein kinase C contains a pseudosubstrate prototope in its regulatory domain, Science 238 (1987) 1726–1728.
[16] L. Theodore, D. Derossi, G. Chassaing, B. Llirbat, M. Kubes, P. Jordan, H. Chneiweiss, P. Godement, A. Prochiantz, Intraneuronal delivery of protein kinase C pseudosubstrate leads to growth cone collapse, J. Neurosci. 15 (1995) 7158–7167.
[17] O. Kaidanovich-Beilin, H. Eldar-Finkelman, Peptides targeting protein kinases: strategies and implications, Physiology (Bethesda) 21 (2006) 411–418.

[18] F. Burlina, S. Sagan, G. Bolbach, G. Chassaing, Quantification of the cellular uptake of cell-penetrating peptides by MALDI-TOF mass spectrometry, Angew. Chem. Int. Ed Engl. 44 (2005) 4244–4247.
[19] F. Burlina, S. Sagan, G. Bolbach, G. Chassaing, A direct approach to quantification of the cellular uptake of cell-penetrating peptides using MALDI-TOF mass spectrometry, Nat. Protoc. 1 (2006) 200–205.
[20] A. Ziegler, Thermodynamic studies and binding mechanisms of cell-penetrating peptides with lipids and glycosaminoglycans, Adv. Drug Deliv. Rev. 60 (2008) 580–597.
[21] A. Ziegler, J. Seelig, Binding and clustering of glycosaminoglycans: a common property of mono- and multivalent cell-penetrating compounds, Biophys. J. 94 (2008) 2142–2149.
[22] A. Ziegler, J. Seelig, Contributions of glycosaminoglycan binding and clustering to the biological uptake of the nonamphipathic cell-penetrating peptide WR9, Biochemistry 50 (2011) 4650–4664.
[23] M. Belting, Heparan sulfate proteoglycan as a plasma membrane carrier, Trends Biochem. Sci. 28 (2003) 145–151.
[24] S. Aubry, F. Burlina, E. Dupont, D. Delaroche, A. Joliot, S. Lavielle, G. Chassaing, S. Sagan, Cell-surface thiols affect cell entry of disulfide-conjugated peptides, FASEB J. 23 (2009) 2956–2967.
[25] S. Aubry, B. Aussedat, D. Delaroche, C.Y. Jiao, G. Bolbach, S. Lavielle, G. Chassaing, S. Sagan, F. Burlina, MALDI-TOF mass spectrometry: a powerful tool to study the internalization of cell-penetrating peptides, Biochim. Biophys. Acta 1798 (2010) 2182–2189.
[26] P. Joanne, C. Galanth, N. Goasdoue, P. Nicolas, S. Sagan, S. Lavielle, G. Chassaing, C. El Amri, I.D. Alves, Lipid reorganization induced by membrane-active peptides probed using differential scanning calorimetry, Biochim. Biophys. Acta 1788 (2009) 1772–1781.
[27] R.M. Epand, R.F. Epand, Lipid domains in bacterial membranes and the action of antimicrobial agents, Biochim. Biophys. Acta 1788 (2009) 289–294.
[28] A. Walrant, I. Correia, C.Y. Jiao, O. Lequin, E.H. Bent, N. Goasdoue, C. Lacombe, G. Chassaing, S. Sagan, I.D. Alves, Different membrane behaviour and cellular uptake of three basic arginine-rich peptides, Biochim. Biophys. Acta 1808 (2011) 382–393.
[29] A. Latal, G. Degovics, R.F. Epand, R.M. Epand, K. Lohner, Structural aspects of the interaction of peptidyl-glycylleucine-carboxyamide, a highly potent antimicrobial peptide from frog skin, with lipids, Eur. J. Biochem. 248 (1997) 938–946.
[30] K. Lohner, E.J. Prenner, Differential scanning calorimetry and X-ray diffraction studies of the specificity of the interaction of antimicrobial peptides with membrane-mimetic systems, Biochim. Biophys. Acta 1462 (1999) 141–156.
[31] K.J. Hallock, D.K. Lee, A. Ramamoorthy, MSI-78, an analogue of the magainin antimicrobial peptides, disrupts lipid bilayer structure via positive curvature strain, Biophys. J. 84 (2003) 3052–3060.
[32] S. Balayssac, F. Burlina, O. Convert, G. Bolbach, G. Chassaing, O. Lequin, Comparison of penetratin and other homeodomain-derived cell-penetrating peptides: interaction in a membrane-mimicking environment and cellular uptake efficiency, Biochemistry 45 (2006) 1408–1420.
[33] S. Deshayes, M. Morris, F. Heitz, G. Divita, Delivery of proteins and nucleic acids using a non-covalent peptide-based strategy, Adv. Drug Deliv. Rev. 60 (2008) 537–547.
[34] B.C. Lagerholm, G.E. Weinreb, K. Jacobson, N.L. Thompson, Detecting microdomains in intact cell membranes, Annu. Rev. Phys. Chem. 56 (2005) 309–336.
[35] C. Chachaty, D. Rainteau, C. Tessier, P.J. Quinn, C. Wolf, Building up of the liquid-ordered phase formed by sphingomyelin and cholesterol, Biophys. J. 88 (2005) 4032–4044.
[36] T. Pott, M. Paternostre, E.J. Dufourc, A comparative study of the action of melittin on sphingomyelin and phosphatidylcholine bilayers, Eur. Biophys. J. 27 (1998) 237–245.
[37] E.J. Prenner, R.N. Lewis, L.H. Kondejewski, R.S. Hodges, R.N. McElhaney, Differential scanning calorimetric study of the effect of the antimicrobial peptide gramicidin S on the thermotropic phase behavior of phosphatidylcholine, phosphatidylethanolamine and phosphatidylglycerol lipid bilayer membranes, Biochim. Biophys. Acta 1417 (1999) 211–223.
[38] J.R. Brender, U.H. Durr, D. Heyl, M.B. Budarapu, A. Ramamoorthy, Membrane fragmentation by an amyloidogenic fragment of human Islet Amyloid Polypeptide detected by solid-state NMR spectroscopy of membrane nanotubes, Biochim. Biophys. Acta 1768 (2007) 2026–2029.
[39] I.D. Alves, N. Goasdoue, I. Correia, S. Aubry, C. Galanth, S. Sagan, S. Lavielle, G. Chassaing, Membrane interaction and perturbation mechanisms induced by two cationic cell penetrating peptides with distinct charge distribution, Biochim. Biophys. Acta 1780 (2008) 948–959.
[40] H. Duplaa, O. Convert, A.M. Sautereau, J.F. Tocanne, G. Chassaing, Binding of substance P to monolayers and vesicles made of phosphatidylcholine and/or phosphatidylserine, Biochim. Biophys. Acta 1107 (1992) 12–22.
[41] S. Deshayes, M.C. Morris, G. Divita, F. Heitz, Interactions of amphipathic CPPs with model membranes, Biochim. Biophys. Acta 1758 (2006) 328–335.
[42] M. Magzoub, L.E. Eriksson, A. Graslund, Comparison of the interaction, positioning, structure induction and membrane perturbation of cell-penetrating peptides and non-translocating variants with phospholipid vesicles, Biophys. Chem. 103 (2003) 271–288.
[43] B. Christiaens, J. Grooten, M. Reusens, A. Joliot, M. Goethals, J. Vandekerckhove, A. Prochiantz, M. Rosseneu, Membrane interaction and cellular internalization of penetratin peptides, Eur. J. Biochem. 271 (2004) 1187–1197.
[44] W. Zhang, S.O. Smith, Mechanism of penetration of Antp(43–58) into membrane bilayers, Biochemistry 44 (2005) 10110–10118.
[45] M. Lindberg, H. Biverstahl, A. Graslund, L. Maler, Structure and positioning comparison of two variants of penetratin in two different membrane mimicking systems by NMR, Eur. J. Biochem. 270 (2003) 3055–3063.
[46] D.I. Chan, E.J. Prenner, H.J. Vogel, Tryptophan- and arginine-rich antimicrobial peptides: structures and mechanisms of action, Biochim. Biophys. Acta 1758 (2006) 1184–1202.